Suspension Characteristics of Magnetically Suspended Frame in Inertially Stabilized Platform

***Abstract*--Comparing with the normal inertially stabilized platform supported by the mechanical bearing, the inertially stabilized platform suspended by active magnetic bearings has characteristics on minimizing friction and improving control precision. The inner azimuth frame is suspended by active magnetic bearings which are non-contact and elastic levitation method, and the disturbance of external frames can be effectively isolated, so vibration is not transferred from external frames to inner azimuth frame. Therefore, the inertially stabilized platform suspended by active magnetic bearings owns high suspension precision. In addition, the tilting of inner azimuth frame is actively controllable by regulating axial magnetic force. In this article, the characteristics of active magnetic bearings are analyzed, and active controllability and suspension performance of inner azimuth frame are tested, the experimental results indicate that the suspension precision of inner azimuth frame had been improved.**

***Index Terms*—inertially stabilized platform (ISP), active magnetic bearing, inner azimuth frame, suspension precision, active controllability.**

I. INTRODUCTION

As a branch of gyro stabilization equipment, the inertially stabilized platform (ISP) for remote sensing is widely applied in the observation system and photography system such as airborne platform and ship-based platform [1, 2]. In general, the airborne remote sensing system requires the uniform linear motion of flight to achieve real-time imaging with high resolution. However, the flight is often affected by disturbances such as air flow, it causes the flight to vibrate with high order multimode random frequency, and the motion of phase center is not stable, so the quality of imaging will be declined. Therefore, the ISP is used to connect imaging camera with flight to provide airborne imaging camera with stable working environment by effectively isolating disturbances [3-5]. In general, the three-axis ISP is applied to orderly isolate the motion of external roll angle, motion of middle pitch angle and motion of inner attitude angle [6, 7]. Because the optical axis is fixed on azimuth frame, the stability of inner azimuth frame is critical for realizing high-precision control of airborne imaging camera [8], even for the resolution of imaging.

Usually, the azimuth frame is connected with other two frames by the mechanical methods such as gear and bearing, so disturbances are transferred from external frames to azimuth frame, it means that the vibration disturbances can not be effectively isolated. In order to effectively isolate the disturbances of pitch frame and roll frame, one kind of untouched connection and suspension method was investigated. Based on the magnetic suspension technology, the azimuth frame rotor is stably suspended by active magnetic bearings, and the displacement and location of rotor can be actively controllable by regulating winding current of active magnetic bearing [9, 10]. For the ISP, the inner frame rotor can be suspended and controllable by magnetic bearings too [11-13]. Therefore, compared with the mechanical ISP, the ISP with active magnetic bearings can realize disturbances isolation and tilting controllability.

In this article, magnetic suspension technology is applied to support the azimuth frame rotor and isolate the disturbances of other frames. In detail, the dynamic performance of active magnetic bearing in magnetically suspended ISP including radial magnetic force and axial magnetic force are analyzed and tested. And then, the suspension precision and tilting controllability of azimuth frame are verified.

II. MAGNETICALLY SUSPENDED ISP

The ISP supported by active magnetic bearings is shown as Fig.1, the whole system consists of roll frame, pitch frame, azimuth frame, magnetic bearing system, measurement system of rotor displacement, observation load and measurement system of attitude and location (POS and gyro). The roll frame is connected with pitch frame by mechanical bearings and gears, and torque motors are applied to drive the roll frame and pitch frame to control the location and tracking velocity. For the azimuth frame, it is suspended by active magnetic bearings in axial and radial directions, the displacement and location of azimuth frame rotor are measured by the displacement sensor system, and its location is controlled by active magnetic bearings too. The payloads such as camera and POS are installed on the azimuth frame rotor to measure the attitude and location of magnetically suspended ISP.

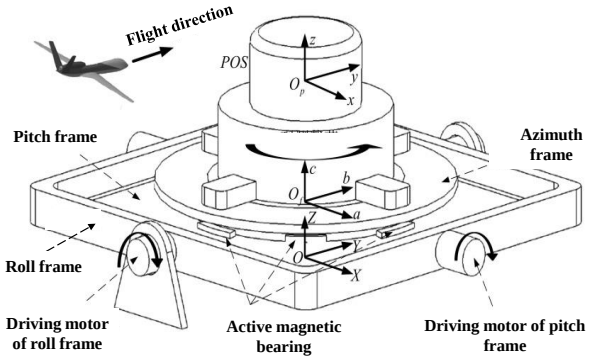

Fig. 1. Structure of magnetically suspended ISP.

III. ACTIVE MAGNETIC BEARING SYSTEM

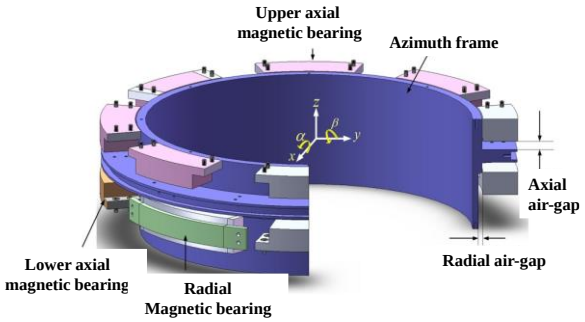

Fig. 2. Structure of active magnetic bearing.

As illustrated as Fig. 2, this kind of active magnetic bearing including the radial magnetic bearing and axial magnetic bearing is designed to keep the azimuth frame of ISP suspended stably in radial and axial directions. Four radial magnetic bearings located at left and right sides of azimuth frame realize the radial suspension of azimuth frame rotor. Eight axial magnetic bearings are located at the upper surface of azimuth frame in axial direction, and four axial magnetic bearings are mounted on lower surface. The four pairs of axial magnetic bearings between the upper surface and lower surface not only control the axial translation of azimuth frame rotor, but also control the tilting of azimuth frame rotor around X and Y axis, the other four upper axial magnetic bearings are only applied to counteract the gravity of azimuth frame rotor. As a consequent, the suspension of azimuth frame rotor on five degree of freedom is realized.

A. *Suspension of Axial Magnetic Bearing*

Axial magnetic bearing needs the great loading ability to counteract the gravity of azimuth frame rotor, but the mass of ISP is limited, the active magnetic bearing should have small volume. Therefore, one kind of asymmetric permanent magnet (PM) biased magnetic bearing is applied in Fig. 3, the biased magnetic flux are not equal in the each load channel. When the upper biased magnetic flux increases, the lower biased magnetic flux decreases, and four pairs of magnetic bearings control the tilting of rotor. When the rotor locates at the equilibrium point, the biased magnetic flux of PM generate magnetic force in the axial direction to counteract gravity, so the control current is decreased. Furthermore, the area of electromagnetic circuit will be reduced, and the total mass of axial magnetic bearing will decrease.

1. *Analysis of Axial Magnetic Force*

The single axial magnetic bearing and its magnetic path is shown as Fig. 4. The PM path passes through internal magnetic ring, air-gap and external magnetic ring. The electromagnetic (EM) path passes through the internal magnetic ring, secondary air-gap, external magnetic ring and air-gap. The equivalent magnetic circuits are shown as Fig. 5. So the equivalent magnetic flux of PM path is

$$\begin{cases} \phi_{pmz+} = F_{pmz+} \Big/ \left(R_{pmsum} \cdot \sigma_p \right) \\ \phi_{pz+} = \phi_{pmz+} \cdot \left(R_{pmsum} - R_{pmz+} \right) \Big/ R_{z+} \\ \phi_{pm} = \phi_{pmz+} \cdot \left(R_{pmsum} - R_{pmz+} \right) \Big/ \left(R_{ez+} + R_{iz+} \right) \end{cases} \tag{1}$$

where ϕ_{pmz+} is the total magnetic flux of PM path, $F_{pmz+} = H_c h_{pm}$ the magnetic force of PM, H_c the coercive force of PM, h_{pm} the magnetization length of PM, σ_p the leakage coefficient.

The magnet reluctance of PM path in every channel is

$$R_{pmsum} = R_{pmz+} + 1 \Big/ \left(\frac{1}{R_{z+}} + \frac{1}{R_{ez+} + R_{iz+}} \right) \tag{2}$$

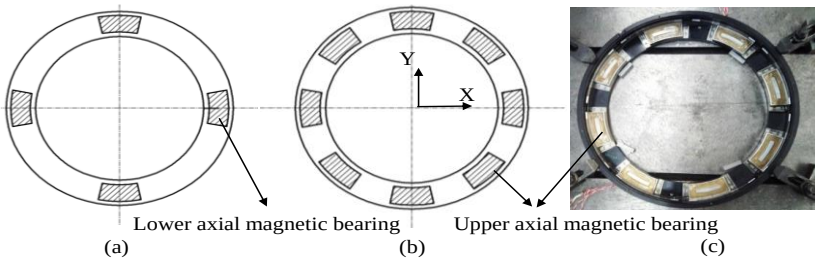

Fig. 3. Axial magnetic bearing, (a) upward view, (b) top view, (c) material object.

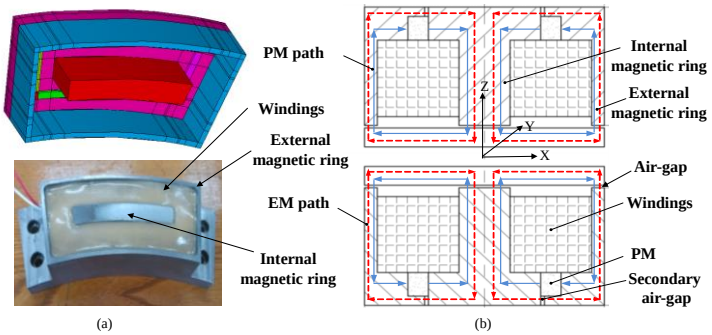

Fig. 4. Single axial magnetic bearing, (a) configuration, (b) magnetic path.

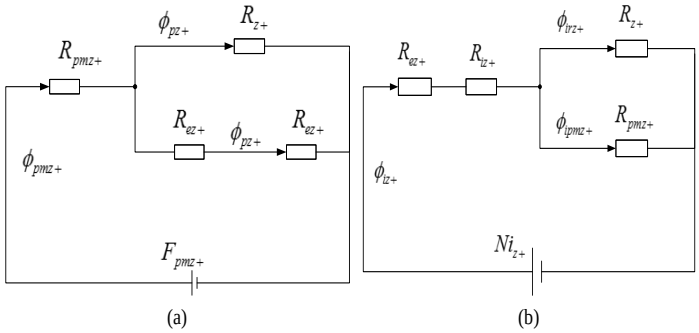

Fig. 5. Equivalent magnetic circuits of axial MB, (a) PM path, (b) EM path.

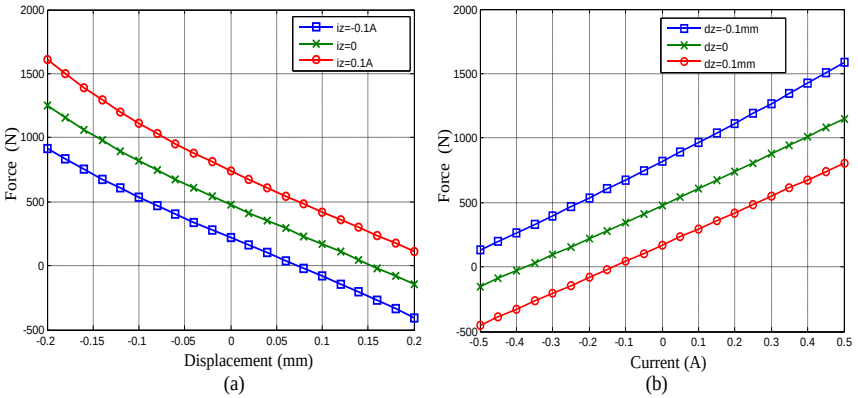

Fig. 6. Magnetic force of axial magnetic bearing, (a) f_z versus d_z, (b) f_z versus i_z.

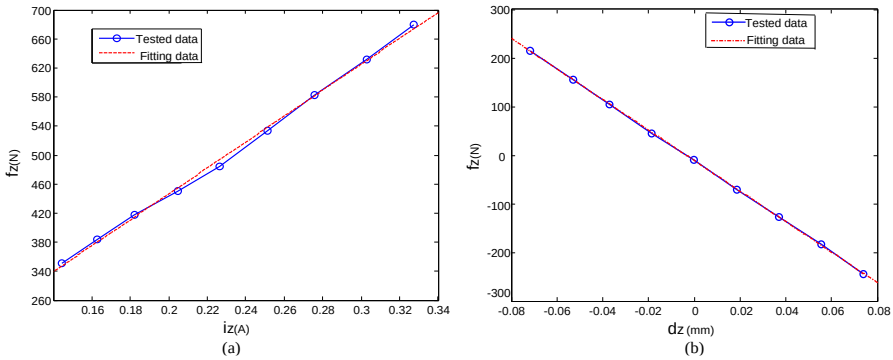

Fig. 7. Tested result of axial magnetic force, (a) f_z versus i_z, (b) f_z versus d_z.

And

$$\begin{cases} R_{pmz+} = h_{pm} / \mu_0 \mu_r A_{pm} \\ R_{z+} = \delta_1 / \mu_0 A_{11} \\ R_{ez+} = \delta_{ez+} / \mu_0 A_{ez+} \\ R_{iz+} = \delta_{iz+} / \mu_0 A_{iz+} \end{cases} \tag{3}$$

where μ_r is the relative permeability of PM, μ_0 the vacuum permeability, A_{pm} the sectional area of PM, A_{ez+} the sectional area of external magnetic ring, A_{iz+} the sectional area of internal magnetic ring, A_{11} the sectional area of secondary air-gap, δ length of air-gap.

For EM path as shown as Fig.6 (b), EM flux is

$$\begin{cases} \phi_{iz+} = Ni_{z+} / \left(R_{isumz+} \sigma_e \right) \\ \phi_{irz+} = \phi_{iz+} \cdot \left(R_{isumz+} - R_{ez+} - R_{iz+} \right) / R_{z+} \\ \phi_{ipmz+} = \phi_{iz+} \cdot \left(R_{isumz+} - R_{ez+} - R_{iz+} \right) / R_{pmz+} \end{cases} \tag{4}$$

where Ni_{z+} is the ampere-turns of winding, i_{z+} the current, σ_z leakage coefficient of EM flux, and magnet flux of EM path $\phi_{z+} = \phi_{pmz+} + \phi_{iz+}$, and magnet reluctance of EM path is

$$R_{isumz+} = R_{ez+} + R_{iz+} + 1 \Big/ \left(\frac{1}{R_{z+}} + \frac{1}{R_{pmz+}} \right) \tag{5}$$

Magnetic forces of upper axial magnetic bearing are

$$\begin{cases} f_{iz+} = \phi_{z+}^2 / \left(2\mu_0 A_{iz+} \right) \\ f_{ez+} = \phi_{z+}^2 / \left(2\mu_0 A_{ez+} \right) \end{cases} \tag{6}$$

where f_{iz+} and f_{ez+} are magnetic forces of upper internal and external stator, respectively. And magnetic forces of lower axial magnetic bearing are

$$\begin{cases} f_{iz-} = \phi_{z-}^2 / (2\mu_0 A_{iz-}) \\ f_{ez-} = \phi_{z-}^2 / (2\mu_0 A_{ez-}) \end{cases} \quad (7)$$

The resultant force of axial magnetic bearing is

$$f_z = (f_{iz+} + f_{ez+}) \times 8 - (f_{iz-} + f_{ez-}) \times 4 \quad (8)$$

Then, magnetic forces in Z axis is

$$f_z = k_{iz} i_z + k_{dz} d_z \quad (9)$$

where k_{iz} is the current stiffness, k_{dz} is the displacement stiffness.

TABLE. I

PARAMETERS OF AXIAL MAGNETIC BEARING

Symbol	Quantity	Value
δ	Length of air gap	0.5mm
H_c	Coercive force of PM	760A/m
N	Turns of axial windings	220
σ_p	Leakage coefficient of PM flux	1.4
σ_e	Leakage coefficient of EM flux	1.05
A_{ez+}	Area of external magnetic ring	52.78mm^2
A_{iz+}	Area of internal magnetic ring	50.75mm^2
h_{pm}	Height of PM	mm
ϕ_{z+}	Total magnetic flux	1.0T

Based on designed parameters of the axial magnetic bearing in TABLE. I, the force-displacement and force-current characteristics are illustrated in Fig. 6. The axial magnetic force is proportional to the displacement and control current when rotor works at the equilibrium position. And the displacement stiffness and current stiffness of axial magnetic bearing is -3200N/mm and 2122N/A, respectively.

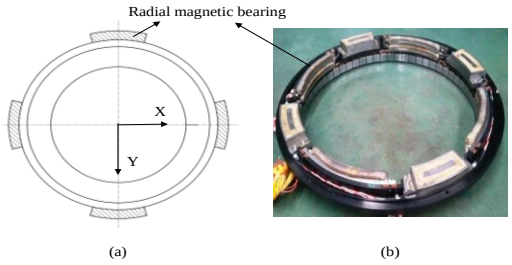

Fig. 8. Radial magnetic bearing, (a) top view, (b) object

2. Tested Result of Axial Magnetic Force

When the azimuth frame rotor is suspended at the radial equilibrium point, different payloads are imposed on azimuth frame rotor in axial direction, the control current of windings generate magnetic force to maintain the rotor suspend at the axial equilibrium point. Then, the relationship between f_z and i_z is shown as Fig. 7 (a), and the axial current stiffness is about 2000 N/A. When there is no payload imposed on azimuth frame rotor in axial direction, through changing the location of azimuth frame rotor, the relationship between f_z and i_z is illustrated as Fig. 7 (b), and the axial displacement stiffness is about -3000N/mm.

B. Suspension of Radial Magnetic Bearing

In the magnetically suspended ISP, the radial magnetic bearing is applied to suppress the radial disturbance force and radial component of gravity when the azimuth frame rotor tilts. Because the azimuth frame is plat thin ring with great diameter as shown as Fig. 8, the independent single channel magnetic bearing is used to reduce the circular span of the radial magnetic bearing in X and Y directions.

1. Analysis of Radial Magnetic Force

The equivalent magnetic circuit of radial magnetic bearing in X+ direction is shown as Fig. 10. As similar to the axial magnetic force, the resultant force in X and Y direction are

$$\begin{cases} f_x = f_{x+} - f_{x-} \\ f_y = f_{y+} - f_{y-} \end{cases} \quad (10)$$

And the magnetic force in X direction and Y direction can be linearized as

$$\begin{cases} f_x = k_{ix} i_x + k_{dx} d_x \\ f_y = k_{iy} i_y + k_{dy} d_y \end{cases} \quad (11)$$

where k_{ix} is the current stiffness in X direction, k_{dx} the displacement stiffness in X direction, k_{iy} the current stiffness in Y direction, k_{dy} the displacement stiffness in Y direction.

According to designed parameters of the radial magnetic bearing listed in TABLE. II, the force-displacement and force-current characteristics are shown in Fig. 11. When azimuth frame rotor works at the axial equilibrium point, the displacement stiffness and current stiffness of radial magnetic bearing is -500N/mm and 320N/A, respectively.

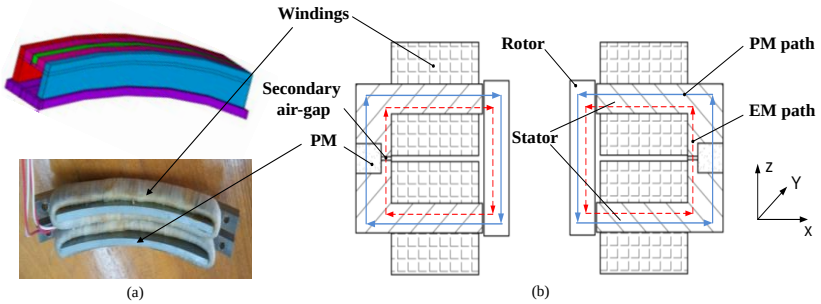

Fig. 9. Magnetic path of radial magnetic bearing, (a) single magnetic bearing, (b) magnetic path.

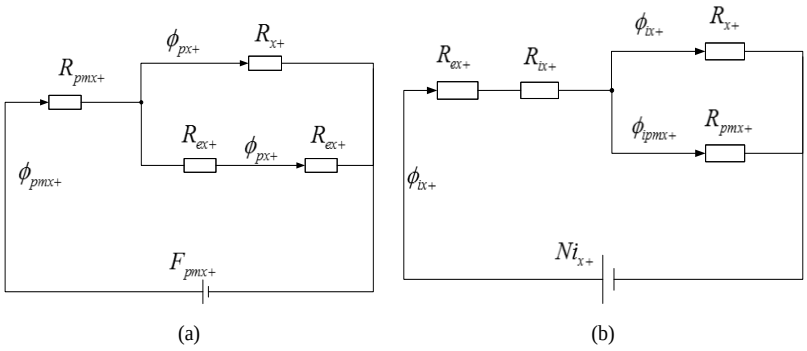

(a) (b)

Fig. 10. Equivalent magnetic circuit of radial magnetic bearing, (a) PM circuit, (b) EM circuit.

2. *Tested Result of Radial Magnetic Force*

TABLE. II

PARAMETERS OF RADIAL MAGNETIC BEARING

Symbol	Quantity	Value
δ_{x+}	Length of air gap	0.4 mm
h_{pm}	Height of PM	5.8 mm
H_c	Coercive force of PM	760 A/m
N_x	Turns of radial windings	220
σ_p	Leakage coefficient of PM flux	1.4
σ_e	Leakage coefficient of EM flux	1.05
A_{x+}	Area of radial magnetic ring	$50mm^2$
ϕ_{x+}	Total magnetic flux	0.49 T

When the azimuth frame rotor is suspended at the axial equilibrium position, the external force is imposed on the azimuth frame rotor in X+ direction, and radial magnetic bearings generate magnetic force to ensure azimuth frame rotor suspended at the equilibrium point. Then, the relationship between the force and control current is illustrated as Fig. 12(a). Further, no external force is acting on azimuth frame rotor, it is suspended at different positions in X axis by regulating the control current, and in order to sustain the stable suspension of azimuth frame rotor, the magnetic bearing generate magnetic force to suppress the influence brought by the displacement. The relationship between the displacement and control current is shown as Fig. 12 (b). When $f_x = 0$, the relationship between displacement stiffness and current stiffness is

$$k_{ix} = -k_{dx} \cdot i_x / d_x \tag{12}$$

where i_x / d_x is the curvature in Fig. 12(b), so the displacement stiffness is

$$k_{dx} = -k_{ix} \cdot d_x / i_x \tag{13}$$

As a result, the current stiffness in radial direction is about 300N/mm, and displacement stiffness is about -480N/A.

IV. DYNAMIC CHARACTERISTICS OF MAGNETICALLY SUSPENDED ISP

A. *Modeling of Magnetically Suspended ISP*

When the inner azimuth frame is levitated by the active magnetic bearings, the force acting on the azimuth frame is illustrated as Fig. 13. f_{z1}, f_{z2}, f_{z3} and f_{z4} are axial magnetic forces to levitate the azimuth frame rotor in axial direction, f_{lx+}, f_{lx-} are magnetic forces generated by upper axial magnetic bearing to control the tilting around Y axis, f_{ly+} and f_{ly-} control the tilting of rotor around X axis. f_{x+} and f_{x-} are magnetic forces generated by radial magnetic bearing in X direction, the suspension in Y axis is controlled by f_{y+} and f_{y-}. β is the tilting angle around Y axis, α is the tilting angle around X axis. So the equation of motion is

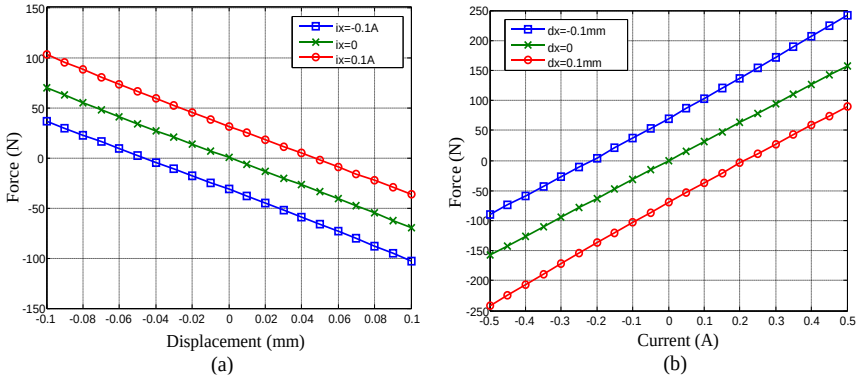

(a) (b)

Fig. 11. Magnetic force of radial magnetic bearing, (a) f_x versus d_x, (b) f_x versus i_x.

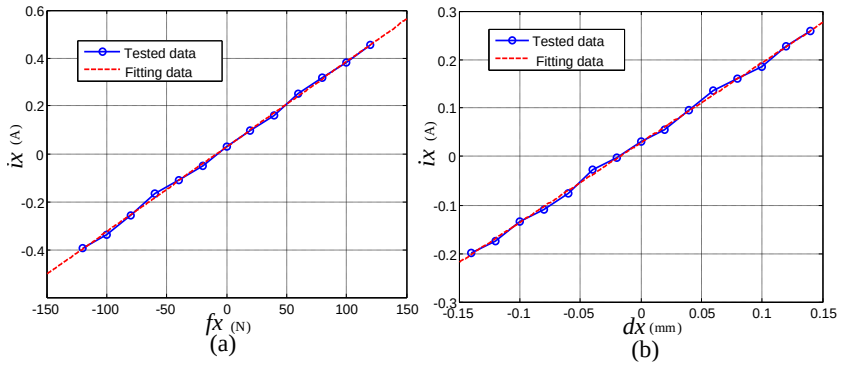

Fig. 12. Tested force of radial magnetic force, (a) f_x versus i_x, (b) d_x versus i_x.

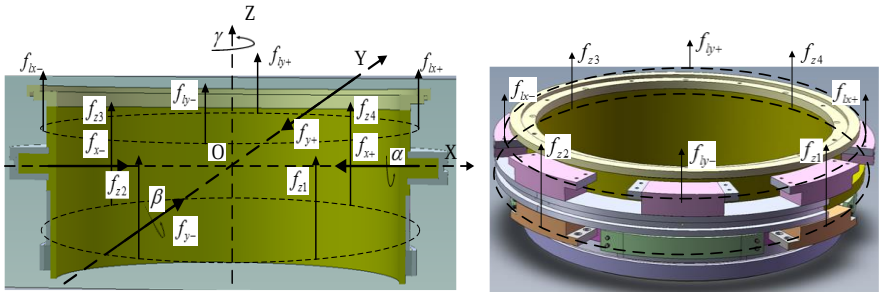

Fig. 13. Force analysis of magnetically suspended frame.

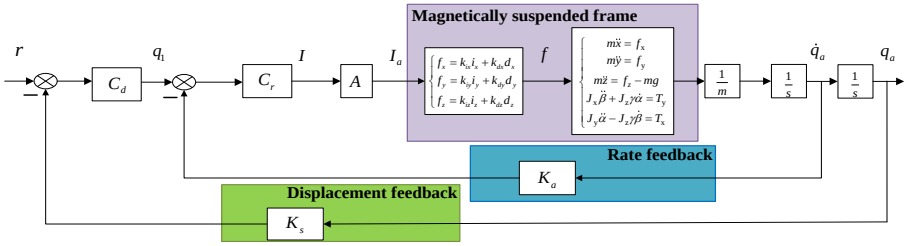

Fig. 14. Control scheme of magnetically suspended ISP.

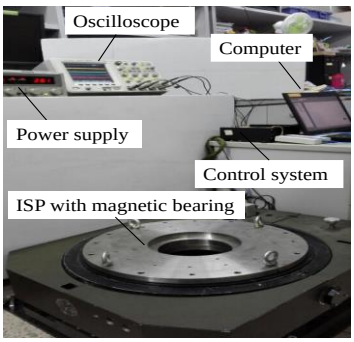

Fig. 15. Experimental setup.

$$\begin{cases} m\ddot{x} = f_x \\ m\ddot{y} = f_y \\ m\ddot{z} = f_z - mg \\ J_x\ddot{\beta} + J_z\gamma\dot{\alpha} = T_y \\ J_y\ddot{\alpha} - J_z\gamma\dot{\beta} = T_x \end{cases} \tag{14}$$

where J_x, J_y and J_z is the moment of inertia around X axis, Y axis and Z axis, T_m the torque of motor, T_y and T_x is the moment around Y axis and X axis generated by two pairs of upper axial magnetic bearing, respectively,

$$\begin{cases} T_y = (f_{lx+} - f_{lx-}) \cdot l \\ T_x = (f_{ly+} - f_{ly-}) \cdot l \end{cases} \tag{15}$$

where l is the distance between one pair of upper axial magnetic bearings. According to the dynamic model of azimuth frame rotor, the control system is shown as Fig. 14, PID control is applied to realize the active control of magnetic suspension system. Whole control system consists of inner control loop of magnetic bearing and outer control loop of azimuth frame. t r is the reference displacement. Through the amplifier matrix A, the control current I is amplified into current I_a, it generates magnetic force. For the rate feedback loop of magnetic bearing, the rates of azimuth frame relative to external frame are measured and feedback in control loop. In the control loop of azimuth frame, the attitude and position of azimuth frame rotor are measured by displacement sensors.

B. Axial Suspension Characteristics of Azimuth Frame Rotor

The experimental setup with magnetically suspended ISP is shown in Fig. 15, a digital signal processor TMS320F28335 with 12-bit A/D converter is used to control the magnetic bearing system, the digital PWM amplifier with 20KHz is applied to drive the magnetic bearing, and

eddy current sensor is used to measure the displacement of azimuth frame rotor, and sensitivity of displacement sensors is 7 V/mm. The sampling frequency of whole control system is stetted as 20KHz and the power supply of whole control system is 28V. The rotor mass is 23kg, Distance between axial magnetic bearings is 520 mm, and Distance between axial sensors is 470 mm.

The suspension of azimuth frame rotor in Z axis is shown as Fig. 16, and the axial static suspension precision of azimuth frame rotor is illustrated as Fig.17. When the azimuth frame rotor is suspended stably, the maximum excursion in axial direction is $2\mu m$, the maximum tilting angle around X axis and Y axis is 0.015mrad, which means that the maximum excursion in the air-gap is only 0.7% of protective gap.

C. *Radial Suspension Characteristic of Azimuth Frame Rotor*

As shown as Fig. 18, the radial magnetic force makes the azimuth frame levitated at the radial equilibrium point, the black solid line illustrates the displacement in X axis measured by sensor x_- and sensor x_+, the green dashed line is the displacement in Y axis. For the static suspension in radial direction, the displacement excursion is shown as Fig.19. When the azimuth frame rotor is suspended stably in radial direction, the maximum excursion is about $4.3\mu m$, which is about 0.86% of radial protective gap.

D. *.Radial Tilting Characteristic of Azimuth Frame Rotor*

Moreover, to demonstrate that the tilting of azimuth frame rotor is actively controllable, sinusoidal signal with maximum 0.1mm and period 0.1s is chosen as reference input, displacements of azimuth frame rotor are measured by one pair of sensors (sensor Z_1 and sensor Z_3), and responses of azimuth frame rotor are shown as Fig. 20(a). When the reference input is the step signal with maximum 0.15mm and minimum -0.1mm, the response of azimuth frame rotor is illustrated as Fig. 20(b). Therefore, the active controllability of axial magnetic bearings are verified.

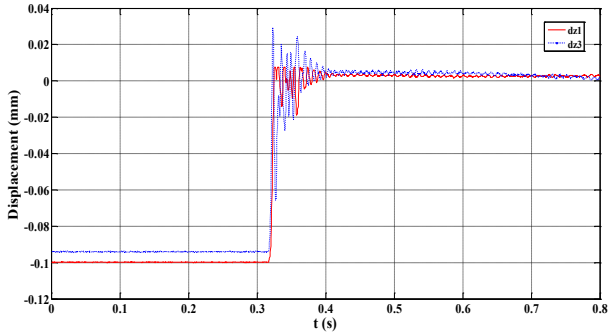

Fig. 16. Axial suspension of azimuth frame rotor

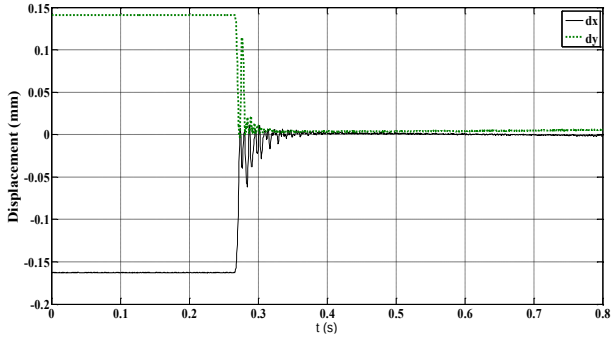

Fig. 18. Radial suspension of azimuth frame rotor.

E. *Vibration Isolation of Magnetically Suspended ISP*

When the magnetically suspended azimuth frame is suspended by active magnetic bearings, the base plate of ISP is stimulated by the sine vibration $r = 3 \cdot \sin(0.2\pi t)$ as illustrated as Fig. 21 (a), and Fig. 21 (b) is the angle displacement of pitch frame (mechanical frame) and azimuth frame measured by positioning orientation system. For the pitch frame, the RMS of angle displacement error is 0.1421°, and RMS of azimuth frame is 0.0712°. It is concluded that the magnetically suspend azimuth frame own better ability of disturbance isolation than the mechanical frames.

V. CONCLUSION

Magnetically suspended ISP is promising to isolate disturbance between the inner azimuth frame and external frames. The characteristic of magnetic bearing in ISP is analyzed based on the equivalent magnetic circuit, and current stiffness and displacement stiffness are measured through regulating the control current and suspension displacement. The dynamic characteristics of inner azimuth frame including tilting and translation are analyzed, and the experimental results demonstrate the magnetic bearing can keep the rotor of inner azimuth frame suspended stably at equilibrium point, the static precision in radial direction is about $4.3\mu m$, and static precision is axial direction is about $2\mu m$, the static tilting precision is about 0.015mrad. Finally, the sinusoidal signal and step signal are imposed on the base plate, and the tilting of azimuth frame rotor is tested, results verify the active controllability of magnetically suspended frame.

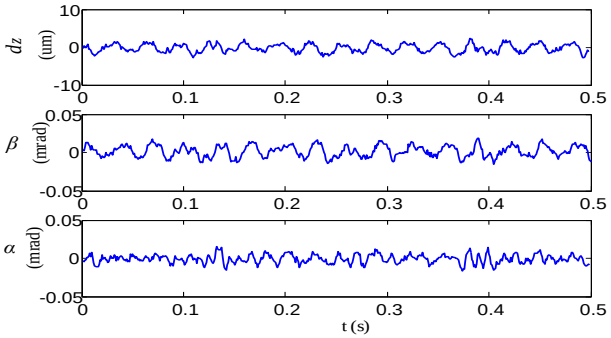

Fig. 17. Static suspension and tilting precision of azimuth frame rotor.

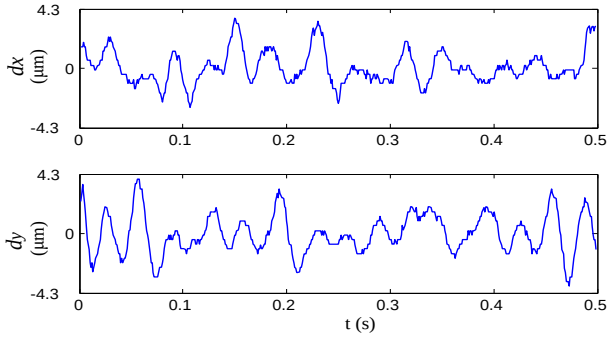

Fig. 19. Radial suspension precision of azimuth frame rotor.

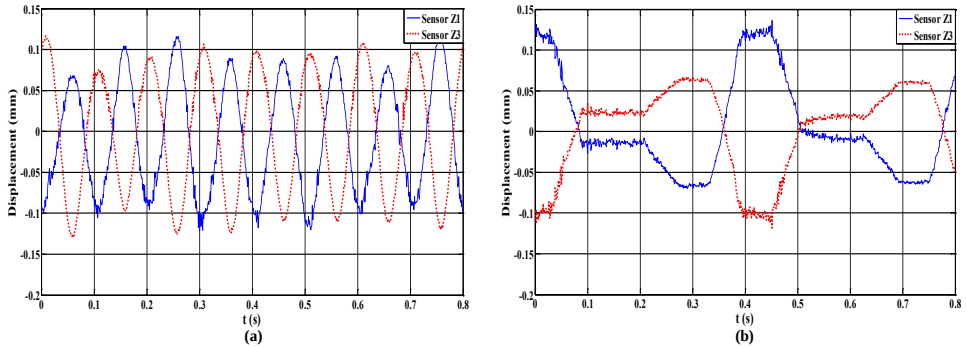

Fig. 20. (a) Sine tilting of azimuth frame rotor, (b) square tilting of azimuth frame rotor.

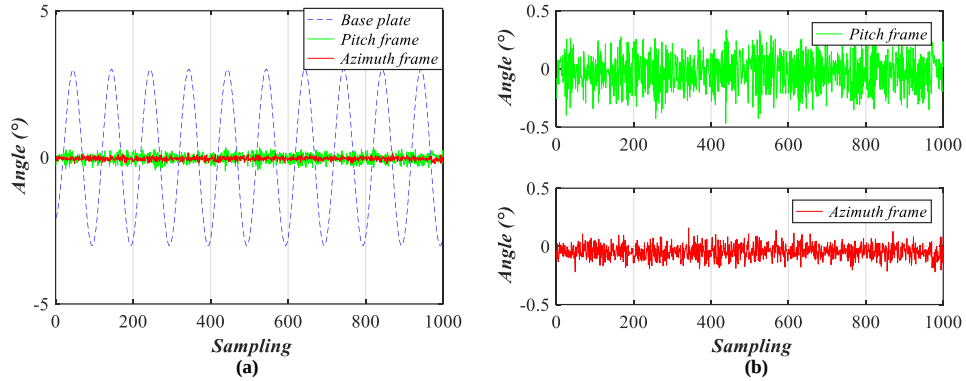

Fig. 21. (a) Vibration of base plate, (b) angle displacement of pitch gimbal and yaw gimbal.

REFERENCES

[1] Z. Hurak and M. Rezac, "Image-based pointing and tracking for inertially stabilized airborne camera platform," *IEEE Transactions on Control Systems Technology,* vol. 20, no. 5, pp. 1146-1159, 2012.

[2] J.-H. Moon and S. Y. Jung, "Implementation of an image stabilization system for a small digital camera," *IEEE Transactions on Consumer Electronics,* vol. 54, no. 2, 2008.

[3] J. Hilkert, "Inertially stabilized platform technology concepts and principles," *IEEE Control Systems,* vol. 28, no. 1, pp. 26-46, 2008.

[4] M. K. Masten, "Inertially stabilized platforms for optical imaging systems," *IEEE Control Systems,* vol. 28, no. 1, pp. 47-64, 2008.

[5] Z. Xiangyang, Y. Ruixia, L. Jianping, and L. Dapeng, "Structure optimal design of roll gimbal for an aerial three-axis ISP based on FEM modal analysis," in *Measuring Technology and Mechatronics Automation (ICMTMA), 2011 Third International Conference on*, 2011, vol. 3, pp. 373-376: IEEE.

[6] J. Hilkert and B. Pautler, "A reduced-order disturbance observer applied to inertially stabilized line-of-sight control," in *Acquisition, Tracking, Pointing, and Laser Systems Technologies XXV*, 2011, vol. 8052, p. 80520H: International Society for Optics and Photonics.

[7] X. Zhou, H. Zhang, and R. Yu, "Decoupling control for two-axis inertially stabilized platform based on an inverse system and internal model control," *Mechatronics,* vol. 24, no. 8, pp. 1203-1213, 2014.

[8] H. F. Mokbel, L. Q. Ying, A. A. Roshdy, and C. G. Hua, "Modeling and optimization of electro-optical dual axis inertially stabilized platform," in *Optoelectronics and Microelectronics (ICOM), 2012 International Conference on*, 2012, pp. 372-377: IEEE.

[9] J. Tang, B. Xiang, and Y. Zhang, "Dynamic characteristics of the rotor in a magnetically suspended control moment gyroscope with active magnetic bearing and passive magnetic bearing," *ISA transactions,* vol. 53, no. 4, pp. 1357-1365, 2014.

[10] B. Xiang and J. Tang, "Suspension and titling of vernier-gimballing magnetically suspended flywheel with conical magnetic bearing and Lorentz magnetic bearing," *Mechatronics,* vol. 28, pp. 46-54, 2015.

[11] Z. Lin and K. Liu, "Inertially stabilized line-of-sight control system using a magnetic bearing with vernier gimbaling capacity," in *Optical Design and Testing VI*, 2014, vol. 9272, p. 92720Q: International Society for Optics and Photonics.

[12] J. Fang, C. Wang, and T. Wen, "Design and optimization of a radial hybrid magnetic bearing with separate poles for magnetically suspended inertially stabilized platform," *IEEE Transactions on Magnetics,* vol. 50, no. 5, pp. 1-11, 2014.

[13] Q. Mu, G. Liu, and X. Lei, "A RBFNN-based adaptive disturbance compensation approach applied to magnetic suspension inertially stabilized platform," *Mathematical Problems in Engineering,* vol. 2014, 2014.